NACA

RESEARCH MEMORANDUM

DYNAMIC LONGITUDINAL STABILITY CHARACTERISTICS OF A

SWEPT-WING FIGHTER-TYPE AIRPLANE AT MACH

NUMBERS BETWEEN 0.36 AND 1.45

By Chester H. Wolowicz

High-Speed Flight Station
Edwards, Calif.

NATIONAL ADVISORY COMMITTEE
FOR AERONAUTICS
WASHINGTON

NATIONAL ADVISORY COMMITTEE FOR AERONAUTICS

RESEARCH MEMORANDUM

DYNAMIC LONGITUDINAL STABILITY CHARACTERISTICS OF A

SWEPT-WING FIGHTER-TYPE AIRPLANE AT MACH

NUMBERS BETWEEN 0.36 AND 1.45

By Chester H. Wolowicz

SUMMARY

As part of the flight research program conducted by the National Advisory Committee for Aeronautics on a swept-wing fighter-type airplane not equipped with an automatic pitch damper, pulse maneuvers were performed at altitudes from 10,000 to 40,000 feet over a Mach number range from 0.36 to 1.45 to determine the longitudinal stability characteristics and derivatives for an original-wing and an extended wing-tip configuration.

The longitudinal dynamic behavior of the airplane during simulated combat maneuvers at altitudes of 30,000 to 40,000 feet was not considered satisfactory, especially at supersonic speeds, because of insufficient pitch damping.

The addition of the wing-tip extensions caused a slight favorable shift in the aerodynamic center of the airplane. The static margin of the extended wing-tip configuration is of the order of 12-percent mean aerodynamic chord in the subsonic region and 29-percent mean aerodynamic chord at Mach numbers above 1.2.

Wind-tunnel data for the two wing configurations investigated showed good agreement with transonic flight results for the lift-curve slope and the static stability derivative C_{m_α}; poor agreement was evident in the supersonic region.

INTRODUCTION

The static and dynamic longitudinal stability characteristics and derivatives, as determined from flight pulse data, for two wing configurations of a 45° swept-wing fighter-type airplane capable of flight well into the supersonic region are presented in this paper. Stabilizer pulse data employed were obtained for an original-wing configuration and also for a configuration with a 1-foot extension of the wing tip. All data were obtained within the 10,000- and 40,000-foot levels over the Mach number range from 0.36 to 1.45 at the NACA High-Speed Flight Station at Edwards, Calif.

The results of the flight data analysis are compared with available wind-tunnel data which have been corrected for the momentum effects of the intake air of the jet engine.

This paper constitutes one part of a general flight investigation of the stability, performance, and aerodynamic load characteristics of the airplane. Results of some other investigations have been reported in references 1 to 4.

SYMBOLS AND COEFFICIENTS

a_n normal acceleration, g units

c wing chord, ft

$\bar{c}$ mean aerodynamic chord, ft

C_L lift coefficient, $\dfrac{\text{Lift}}{1/2\rho V^2 S}$

C_{L_α} lift-curve slope $\dfrac{\partial C_L}{\partial \alpha}$, per radian in equations, per deg in figures

$C_{L_{\dot{\alpha}}}$ $\dfrac{\partial C_L}{\partial\left(\dfrac{\dot{\alpha}\bar{c}}{2V}\right)}$, per radian

C_{L_q} $\dfrac{\partial C_L}{\partial\left(\dfrac{q\bar{c}}{2V}\right)}$, per radian

C_m pitching-moment coefficient, $\dfrac{\text{Pitching moment}}{1/2\rho V^2 S \bar{c}}$

$C_{m_{C_L}}$ static margin, mean chord units

C_{m_α} longitudinal stability derivative $\dfrac{\partial C_m}{\partial \alpha}$, per radian in equations, per deg in figures

$C_{m_{\dot\alpha}}$ $\dfrac{\partial C_m}{\partial\left(\dfrac{\dot\alpha \bar{c}}{2V}\right)}$, per radian

C_{m_q} $\dfrac{\partial C_m}{\partial\left(\dfrac{q \bar{c}}{2V}\right)}$, per radian

g acceleration of gravity, ft/sec^2

h_p pressure altitude, ft

I_Y moment of inertia of airplane relative to pitch axis, slug-ft^2

i_t horizontal stabilizer deflection, positive direction when nose of stabilizer is up, deg

m mass of airplane, $\dfrac{W}{g}$, slugs

M Mach number

P period of damped natural frequency of airplane, sec

q pitch rate of airplane, radians/sec

$\dot q$ pitch acceleration of airplane, radians/sec^2

S wing area, sq ft

$T_{1/2}$ time required for transient oscillation to damp to half amplitude, sec

t time, sec

V   airspeed, ft/sec

W   weight of airplane, lb

α angle of attack of airplane, angle between reference body
                axis and the relative wind, per radian in equations, per
                deg in figures

$\dot{\alpha}$ rate of change of angle of attack with time, radians/sec

δ_{s_i} inboard slat position, percent of fully open position

δ_{s_o} outboard slat position, percent of fully open position

ζ ratio of actual damping to critical damping

ρ mass density of air, slugs/cu ft

AIRPLANE

The test airplane is a fighter-type with a 45° swept wing and a low
horizontal tail. It is powered by a single turbojet engine equipped
with an afterburner. A three-view drawing of the airplane with the orig-
inal vertical tail is shown in figure 1. Figure 1 also shows a dotted
outline of the wing employed in the extended-wing configuration. A photo-
graph of the airplane is shown in figure 2. The wing-tip extensions
were added to increase the static margin and improve the stability for
the external wing-mounted fuel-tank configuration. The airplane was not
equipped with an automatic pitch damper.

The data for the original-wing and extended wing-tip configurations
were obtained with several different vertical tails mounted on the air-
plane at various times during the tests (ref. 4). The effects of the
changes in the vertical tails on the longitudinal stability character-
istics are considered negligible.

The airplane is equipped with automatic leading-edge slats installed
as five interconnected segments. At 40,000 feet, the slats were open at
Mach numbers below 0.84 for steady flight; the slats started to open in
response to air loads at angles of attack of 4°, 5°, 7°, and 8°, at Mach
numbers of 0.84, 0.94, 1.03, and 1.08, respectively. At 20,000 feet, the
slats were open at Mach numbers below 0.72 for steady flight; the slats
started to open at angles of attack of 4° and 6° at Mach numbers of 0.72
and 0.86, respectively.

The physical characteristics of the two configurations are presented in table I. The estimated variation with airplane weight of the moment of inertia relative to the pitch axis (fig. 3) is based on the manufacturer's estimate for design weight and empty weight conditions (ref. 5).

INSTRUMENTATION AND INSTRUMENT ACCURACY

Standard NACA instruments were used to record airspeed, altitude, pitching velocity and acceleration, normal acceleration, angle of attack, control-surface positions, and leading-edge slat positions. The angle of attack, airspeed, and altitude were sensed on the nose boom. All records were synchronized at 0.1-second intervals by a common timing circuit.

The pitch turnmeter used to measure the pitching velocity and acceleration is considered accurate to within ±0.5 percent of range. The turnmeter mounting direction error is 0.5° or less.

The indicated normal accelerometer readings were corrected to the center of gravity. The accelerometer is considered accurate to within ±0.5 percent of range.

The vane-type pickup for measuring the angle of attack was mass balanced and had dynamically flat response characteristics over the frequency range of the airplane. Although the pickup is statically accurate to ±0.1°, the indicated angle of attack has been corrected only for pitching velocity to the center of gravity of the airplane.

The ranges, dynamic characteristics, and scales of recorded data for the angle-of-attack, velocity, and acceleration instruments are:

Quantity	Range	Scale of recorded data (per in. deflection)	Undamped natural frequencies, cps	Damping ratio
α, deg	-20 to 40	10.0 to 10.55	8	0.70
q, radians/sec	±0.5	0.99 to 1.075	7 to 8	0.65
$\dot{q}$, radians/sec^2	±1.0	1.38 to 2.16	14	0.65
a_n, g	-1 to 7	4.48 to 5.93	19	0.55 at 10,000 ft 0.48 at 20,000 ft 0.43 at 30,000 ft 0.38 at 40,000 ft 0.33 at 50,000 ft

Control-surface and leading-edge slat positions were measured by standard control-position transmitters. The control-surface position transmitters were linked directly to the control surfaces and are considered accurate to within ±0.1°.

The nose-boom installation for measuring the airspeed was calibrated by NACA radar phototheodolite method. The Mach numbers presented are considered accurate to ±0.02.

TESTS

The test procedure for this investigation consisted of recording the airplane response to abrupt stabilizer pulses performed with the other controls fixed. In all instances the pilot attempted to maintain constant Mach number and altitude and to prevent movement of the control surfaces during the transient portion of the maneuver. Figures 4(a) and 4(b) present typical time histories.

The stabilizer pulse maneuvers were generally performed at 1g ± 0.1g conditions; however, for the original wing configuration at Mach numbers above M = 1.05 the maneuvers were performed at various load factors and altitudes from 40,000 to 35,000 feet. Pulse maneuvers at Mach numbers greater than 1.35 were performed following a pull-out from a dive. The following table lists the altitudes and corresponding Mach number ranges for which data were obtained for each configuration:

Configuration	Altitude, ft	Mach number range
Original wing	40,000	0.77 to 1.45
Extended wing	40,000	0.79 to 1.26
	30,000	0.53 to 1.03
	10,000	0.36 to 0.93

ANALYSIS

A preliminary study of the data showed no significant nonlinear influences, hence linearized, small disturbance, short-period forms of the longitudinal equations of motion of the airplane constituted the basis of the analysis.

The time-vector method of analysis (refs. 4, 6, 7, and 8) was employed to determine the derivatives. Because of the lack of reliability of the determined values of $\left(C_{L_q} + C_{L_{\dot{\alpha}}}\right)$, this quantity is not presented.

The magnitudes of C_{m_α} and $\left(C_{m_q} + C_{m_{\dot\alpha}}\right)$, as determined by the time-vector method of analysis, were spot-checked by using the following equations and were found to be in agreement.

$$C_{m_\alpha} = -\frac{I_Y}{(1/2\rho V^2)\,S\bar c}\left[\left(\frac{2\pi}{P}\right)^2 + \left(\frac{0.693}{T_{1/2}}\right)^2\right] \tag{1}$$

$$\left(C_{m_q} + C_{m_{\dot\alpha}}\right) = \frac{4 I_Y V}{(1/2\rho V^2)\,S\bar c^2}\left[\frac{C_{L_\alpha}\rho V S}{4m} - \frac{0.693}{T_{1/2}}\right] \tag{2}$$

The original-wing area was employed in analyzing all flight data. To convert the derivatives of the extended-wing configuration to the actual wing area and wing-chord basis, the C_{L_α} derivative should be multiplied by 0.98, C_{m_α} by 0.99, and $\left(C_{m_q} + C_{m_{\dot\alpha}}\right)$ by 1.01.

In fairing the test points to obtain a constant altitude, 1g curve, consideration was given to the influence of altitude and load factor on the test points when the test points were obtained from maneuvers at other than the desired altitude and load factor conditions.

PRESENTATION OF RESULTS

A summary of the figures presenting the results of this investigation is:

Flight data results / Configuration	Trim, α	Period and damping	Static and dynamic longitudinal derivatives	Comparison with rating criteria
Original wing, h_p = 40,000 feet	5	6	7	-
Extended wing, h_p = 10,000, 30,000, 40,000 feet	5	8	10	9
Influence of wing-tip extensions	-	11	12	-

The variation of trim α with Mach number shown in figure 5 for three distinct altitudes has been included not only to show trim α but also to aid in estimating the probability, during the pulse maneuvers, of the automatic opening of the slats when use is made of the information previously presented in the section describing the airplane.

<center>DISCUSSION</center>

<center>Original Wing</center>

On the basis of available data the period curve (fig. 6) shows a smooth and normal large decrease in the Mach number region between 0.85 and 0.95, followed by a more gradual decrease to the highest Mach number. The damping ratio ζ (fig. 6) shows an appreciable decrease in the Mach number region between 0.85 and 0.90. In general, ζ is primarily a function of the air density ρ and the aerodynamic derivatives $\left(C_{m_q} + C_{m_{\dot\alpha}}\right)$, C_{m_α}, and C_{L_α} as shown by the following approximate expression based on approximations of equations (1) and (2):

$$\zeta \approx \sin\left\{\tan^{-1}\left[\sqrt{\frac{\bar{c}3S}{32I_Y}}\sqrt{\frac{\rho}{-C_{m_\alpha}}}\left(\frac{2I_Y C_{L_\alpha}}{m\bar{c}^2} - \left(C_{m_q} + C_{m_{\dot\alpha}}\right)\right)\right]\right\} \tag{3}$$

Thus, the primary causes of the large decrease in the damping ratio in the Mach number region between 0.85 and 0.90 are the large increase in C_{m_α} in the transitional Mach number region and the decrease in $\left(C_{m_q} + C_{m_{\dot\alpha}}\right)$, which are shown in figure 7. In the subsonic region, there is some uncertainty in the value of the damping; therefore, fairing the $T_{1/2}$ points has not been attempted. Insufficient data in this region precluded the possibility of defining a reliable curve.

The magnitudes of C_{L_α} and C_{m_α} and the variation of these derivatives with Mach number (fig. 7) show generally good agreement with wind-tunnel data[1] (ref. 9) which were corrected for the momentum effects of the intake air of the jet engine. It should be pointed out that in the Mach number region between 0.85 and 0.90 there is appreciable scatter of C_{L_α} points, considerably above the experimental scatter, which may be in accordance with the rapid variations with Mach number shown in

---

[1]The horizontal tail of the wind-tunnel model had an NACA 65A007 airfoil section, whereas the airplane had an NACA 65A003.5 airfoil section.

references 10 and 11. It was not possible to verify the presence of the rapid variations in C_{L_α} from a study of available wind-tunnel data because of the lack of wind-tunnel test points within this region.

Extended Wing

The results of the analysis of the data for the extended-wing airplane (figs. 8 and 10) show the same general behavior of the individual quantities plotted as functions of Mach number as was discussed for the original-wing configuration; consequently, detailed consideration of the variation of the quantities with Mach number is omitted.

The decrease in period which occurred with decrease in altitude (fig. 8) is primarily due to the corresponding increase in dynamic pressure, overshadowing the effect of decreasing C_{m_α}, which would tend to increase the period.

If the aerodynamic derivatives of equation 3 were invariant with altitude, the damping ratio ζ could be expected to increase as the altitude is decreased. The increase in ζ with decrease in altitude at subsonic speeds, as shown in figure 8, is considerably less than would be obtained by a change in air density alone. This condition is attributable to the decrease in the magnitude of the damping derivative $\left(C_{m_q} + C_{m_{\dot\alpha}}\right)$ with decreasing altitude.

Pilot opinion indicated that the airplane, which did not have a pitch damper, was unsatisfactory insofar as the longitudinal dynamic behavior was concerned during simulated combat at altitudes varying from 40,000 to 30,000 feet. At supersonic Mach numbers, the airplane had initial rapid and abrupt response to control input followed by prolonged, rapid short-period oscillations. At low subsonic Mach numbers, the airplane had a slow initial response followed by prolonged slow oscillations which required concentration to eliminate. The most acceptable, but still unsatisfactory, characteristics were noticed in the vicinity of $M = 0.8$. The results of the analysis have been plotted on a qualitative rating chart (fig. 9) obtained from reference 12; pilot's opinion showed good qualitative agreement with the criteria of figure 9. Caution should be used in attempting to evaluate the handling qualities of the airplane with any simplified criteria, inasmuch as other factors such as control system characteristics can have an important bearing on the overall airplane response characteristics. Insofar as the Military Specification (ref. 13) for damping characteristics is concerned, the airplane did not meet the specification that a combat airplane damp to one-tenth amplitude

in one cycle (ζ = 0.343). If the airplane is considered to be flying under emergency conditions, as the result of having an inoperative pitch damper, the data of figure 9 imply the airplane would not meet the minimum specification that the airplane damp to one-half amplitude in one cycle (ζ = 0.11) during emergency (damper-inoperative) conditions at combat ceiling, which in this instance is above 50,000 feet. However it was found that the airplane was quite controllable even though not satisfactory as a gun platform.

A comparison of the variation with Mach number of the flight-determined values of C_{L_α} and C_{m_α} for an altitude of 40,000 feet with those determined from unpublished Langley 8-foot high-speed tunnel data (fig. 10) indicates good agreement in the transonic region and poor agreement in the supersonic region.

The decreased magnitude of C_{L_α} with decreased altitude (fig. 10) is possibly due, to some extent, to aeroelastic effects. Although wind-tunnel data do show that the slats cause a small change in the angle of zero lift, the data do not indicate any nonlinearities in the plots of C_L against α within the angle-of-attack range of the flight data; nor do wind-tunnel data and incomplete flight data indicate any significant influence of slats on C_{L_α}.

The C_{m_α} curves (fig. 10) show distinct altitude effects primarily in the region of the transonic aerodynamic-center shift. A study of the unpublished Langley 8-foot high-speed tunnel data in the region of the transonic aerodynamic-center shift for these same altitudes suggests that possibly these are angle-of-attack effects.

The damping derivative $\left(C_{m_q} + C_{m_{\dot\alpha}}\right)$ shows dependency on altitude at any one Mach number for its magnitude in the subsonic region. This influence of altitude is possibly due to aeroelastic deformation of the stabilizer, fuselage, and wing.

Influence of Wing-Tip Extensions

A summary of the results of the analysis for the two wing configurations at an altitude of 40,000 feet is presented in figures 11 and 12 to show the influence of the addition of wing-tip extensions to the original wing. Influences are evident with respect to the period P, the damping ratio ζ, and the derivatives C_{L_α}, C_{m_α}, and $\left(C_{m_q} + C_{m_{\dot\alpha}}\right)$.

The decrease in ζ resulting from the addition of the wing-tip extensions (fig. 11) is attributable primarily to the corresponding negative increase in C_{m_α} and the negative decrease in $\left(C_{m_q} + C_{m_{\dot{\alpha}}}\right)$; the increase in C_{L_α} tends to increase the damping ratio. The reason for the apparent negative decrease in $\left(C_{m_q} + C_{m_{\dot{\alpha}}}\right)$ is not clear, based on available data.

The influence of wing-tip extensions on the static margin is shown in figure 12. The static margin of the original-wing configuration appears to be of the order of $0.10\bar{c}$ at a Mach number of 0.85 and increases to about $0.29\bar{c}$ at a Mach number of 1.03. The measured differences in the static margin resulting from the addition of wing-tip extensions were small and probably within the accuracy of the data. A rough calculation based on simple geometric concepts indicated a $0.03\bar{c}$ increase in static margin due to wing-tip extensions might be expected.

CONCLUSIONS

From the analysis of flight pulse data obtained for an original-wing and an extended wing-tip configuration of a swept-wing fighter-type airplane, not equipped with a pitch damper, over the Mach number range of 0.36 to 1.46, the following conclusions have been reached:

1. The longitudinal dynamic behavior of the airplane during simulated combat maneuvers at altitudes of 30,000 to 40,000 feet was not considered satisfactory, especially at supersonic speeds, because of insufficient pitch damping.

2. The addition of wing-tip extensions resulted in a slight favorable shift in the aerodynamic center of the airplane. The static margin of the wing with tip extensions is of the order of 12-percent mean aerodynamic chord in the subsonic region and 29-percent mean aerodynamic chord at Mach numbers above 1.2.

3. Wind-tunnel data for the two wing configurations investigated showed good agreement with transonic flight results for the lift-curve slope and the static stability derivative C_{m_α}; poor agreement was evident in the supersonic region.

High-Speed Flight Station,
    National Advisory Committee for Aeronautics,
        Edwards, Calif., July 23, 1956.

REFERENCES

1. NACA High-Speed Flight Station: Flight Experience With Two High-
     Speed Airplanes Having Violent Lateral-Longitudinal Coupling in
     Aileron Rolls. NACA RM H55A13, 1955.

2. Finch, Thomas W., Peele, James R., and Day, Richard E.: Flight Invest-
     igation of the Effect of Vertical-Tail Size on the Rolling Behavior
     of a Swept-Wing Airplane Having Lateral-Longitudinal Coupling.
     NACA RM H55L28a, 1956.

3. Drake, Hubert M., Finch, Thomas W., and Peele, James R.: Flight
     Measurements of Directional Stability to a Mach Number of 1.48 for
     an Airplane Tested With Three Different Vertical Tail Configurations.
     NACA RM H55G26, 1955.

4. Wolowicz, Chester H.: Time-Vector Determined Lateral Derivatives of
     a Swept-Wing Fighter-Type Airplane With Three Different Vertical
     Tails at Mach Numbers Between 0.70 and 1.48. NACA RM H56C20, 1956.

5. Weight Control Section, N.A.A.: Airplane Inertia Calculations for
     an Air Superiority Fighter Airplane - Day, (Monoplane), AF Model
     F-100A, (NAA Model NA-192), Contract No. AF33(600)-6545.
     Rep. No. NA-52-185, North American Aviation, Inc., Oct. 1953.

6. Breuhaus, W. O.: Resumé of the Time Vector Method as a Means for
     Analyzing Aircraft Stability Problems. WADC Tech. Rep. 52-299
     (Contract No. AF33(038)-20659 RDO No. 461-1-2) Wright Air Dev.
     Center, U. S. Air Force, Nov. 1952.

7. Larrabee, E. E.: Application of the Time-Vector Method to the Analysis
     of Flight Test Lateral Oscillation Data. FRM No. 189, Cornell
     Aero. Lab. Inc., Sept. 9, 1953.

8. Sternfield, L.: A Vector Method Approach to the Analysis of the
     Dynamic Lateral Stability of Aircraft. Jour. Aero. Sci., vol. 21,
     no. 4, Apr. 1954, pp 251-256.

9. Runckel, Jack F., and Schmeer, James W.: The Aerodynamic Character-
     istics at Transonic Speeds of a Model With a 45° Sweptback Wing,
     Including the Effect of Leading-Edge Slats and a Low Horizontal
     Tail. NACA RM L53J08, 1954.

10. Harris, William G.: A Wind-Tunnel Investigation at High-Subsonic
     and Low Supersonic Mach Numbers on a Series of Wings With Various
     Sweepback, Taper, Aspect Ratio, and Thickness. Part 2. Comparison
     of Lift and Stability Data. AF Tech. Rep. no. 6669. Part 2,
     Wright Air Dev. Center, Dec. 1952.

11. Polhamus, Edward C.: Summary of Results Obtained by Transonic-Bump
    Method on Effects of Plan Form and Thickness on Lift and Drag Char-
    acteristics of Wings at Transonic Speeds. NACA TN 3469, 1955.

12. Harper, Robert P., Jr.: Flight Evaluations of Various Longitudinal
    Handling Qualities in a Variable-Stability Jet Fighter. WADC
    Tech. Rep. 55-299, July 1955.

13. Anon: Military Specification - Flying Qualities of Piloted Airplanes.
    MIL-F-8785 (ASG), Amendment-2, Oct. 17, 1955.

TABLE I

PHYSICAL CHARACTERISTICS OF AIRPLANE

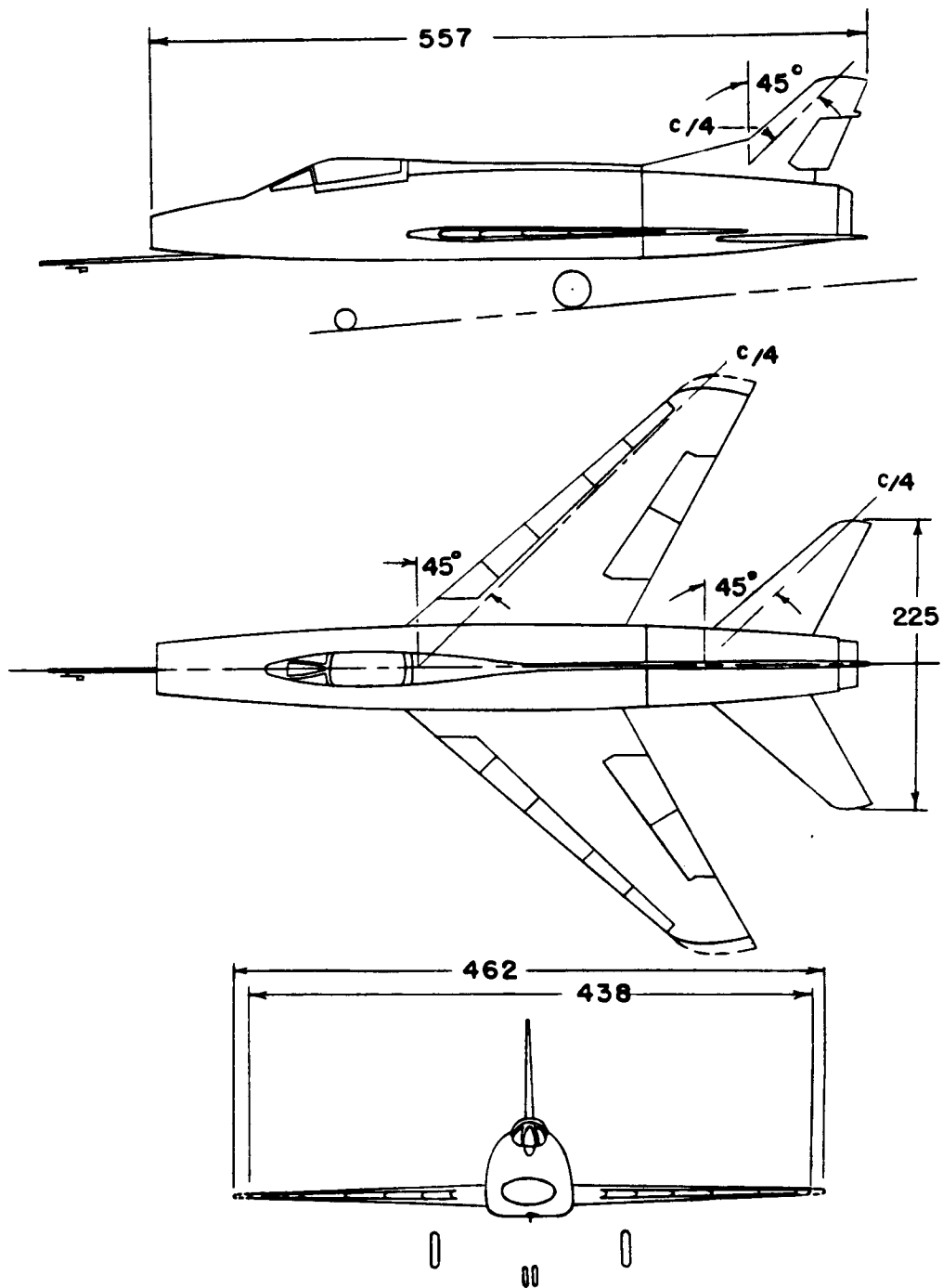|	Original wing	Extended wing
Wing:		
Airfoil section	NACA 64A007	NACA 64A007
Total area (including aileron and 83.84 sq ft covered by fuselage), sq ft	376.02	385.21
Span, ft	36.58	38.58
Mean aerodynamic chord, ft	11.33	11.16
Root chord, ft	15.86	15.86
Tip chord, ft	4.76	4.15
Taper ratio	0.30	0.262
Aspect ratio	3.56	3.86
Sweep at 0.25 chord line, deg	45	45
Incidence, deg	0	0
Dihedral, deg	0	0
Geometric twist, deg	0	0
Aileron:		
Area rearward of hinge line (each), sq ft	19.32	19.32
Span at hinge line (each), ft	7.81	7.81
Chord rearward of hinge line, percent wing chord	25	25
Travel (each), deg	±15	±15
Leading-edge slat:		
Span, equivalent, ft	12.71	12.71
Segments	5	5
Spanwise location, inboard end, percent wing semispan	24.6	23.3
Spanwise location, outboard end, percent wing semispan	94.1	89.2
Ratio of slat chord to wing chord (parallel to fuselage reference line), percent	20	20
Rotation, maximum, deg	15	15
Horizontal tail:		
Airfoil section . . . . NACA 65A003.5		
Total area (including 31.65 sq ft covered by fuselage), sq ft 98.86		
Span, ft 18.72		
Mean aerodynamic chord, ft 5.83		
Root chord, ft 8.14		
Tip chord, ft 2.46		
Taper ratio 0.30		
Aspect ratio 3.54		
Sweep at 0.25 chord line, deg 45		
Dihedral, deg 0		
Travel, leading edge up, deg 5		
Travel, leading edge down, deg 25		
Fuselage:		
Length (afterburner nozzle closed), ft 45.64		
Maximum width, ft 5.58		
Maximum depth over canopy, ft 6.37		
Side area (total), sq ft 230.92		
Fineness ratio (afterburner nozzle closed) 7.86		
Speed brake:		
Surface area, sq ft 14.14		
Maximum deflection, deg 50		
Powerplant:		
Turbojet engine . . . . One Pratt & Whitney J57-P7 with afterburner		
Thrust (guarantee sea level), afterburner, lb 15,000		
Military, lb 9,220		
Normal, lb 8,000		
Airplane weight, lb:		
Basic (without fuel, oil, water, pilot) 19,662		
Total (full fuel, oil, water, pilot) 24,800		
Center-of-gravity location, percent c̄:		
Total weight - gear down 29.5		
Total weight - gear up 29.5		

Figure 1.- Three-view drawing of airplane with original vertical tail
and the extended as well as the original wing. All dimensions in
inches.
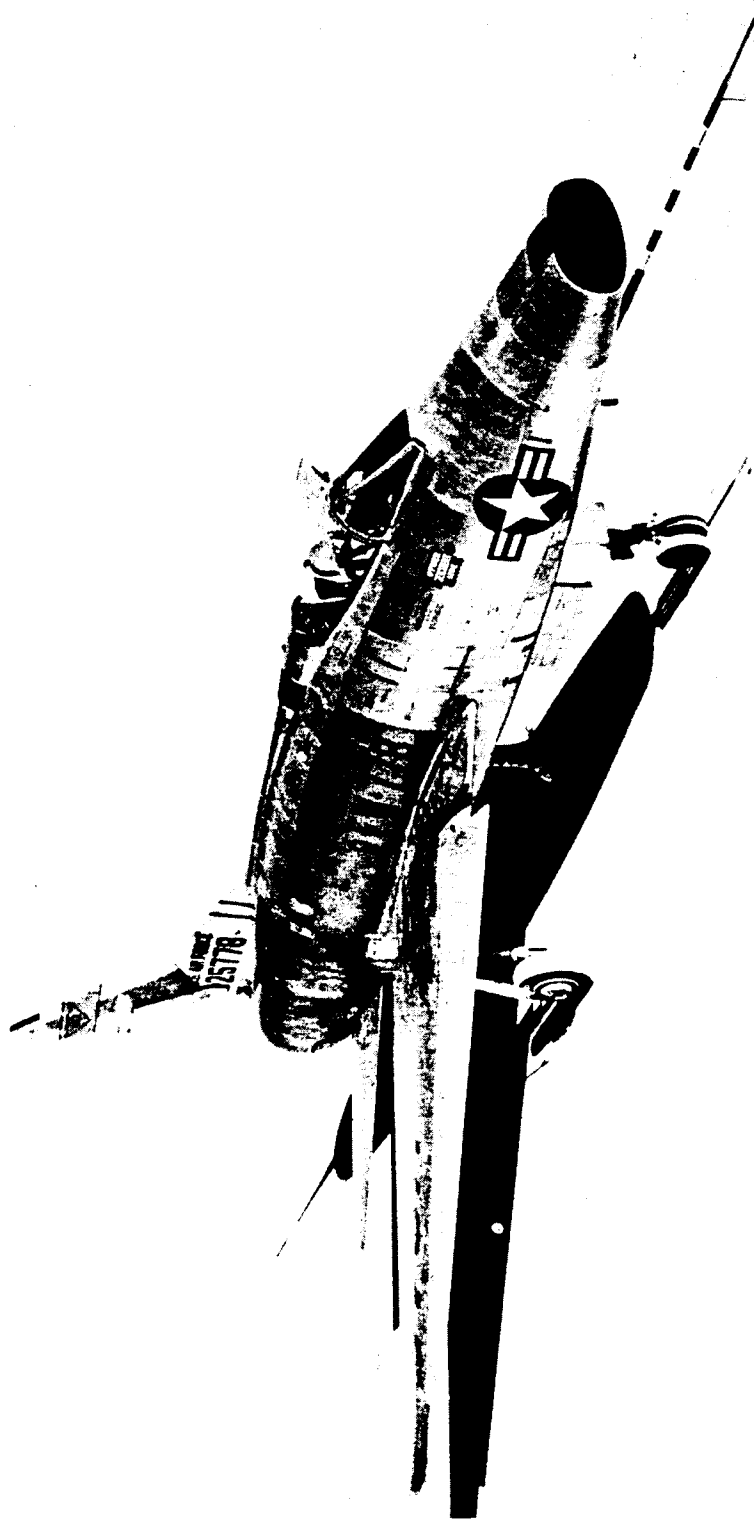
E-2095
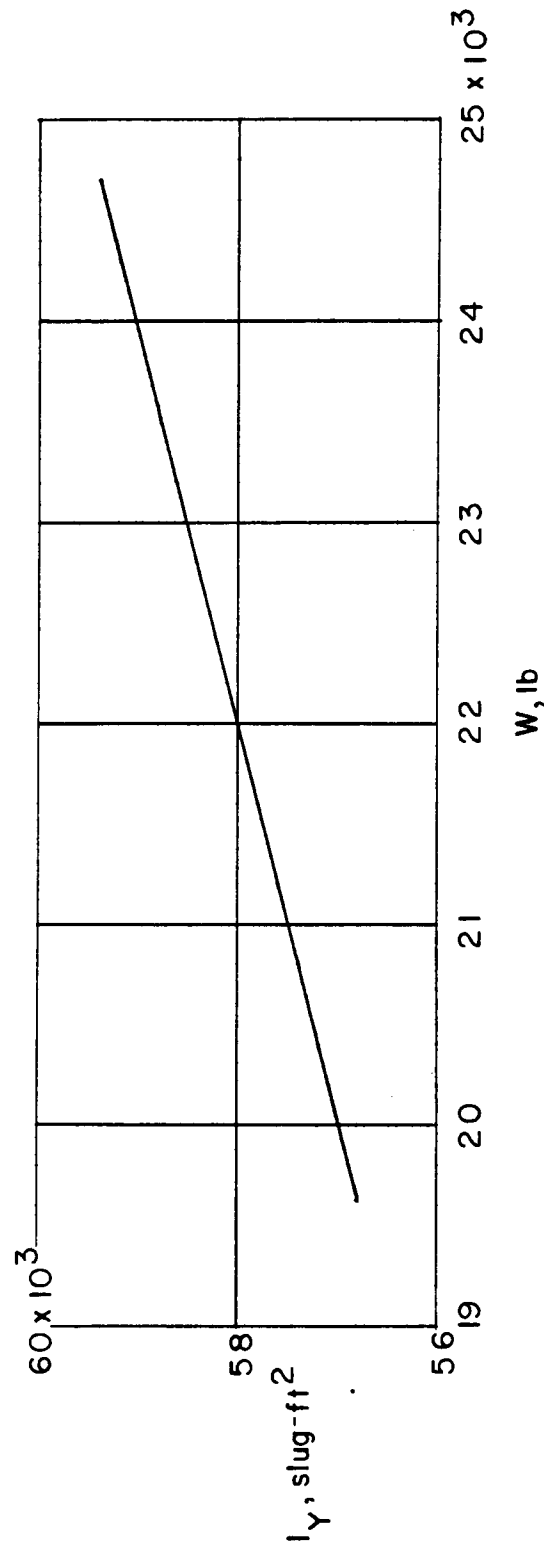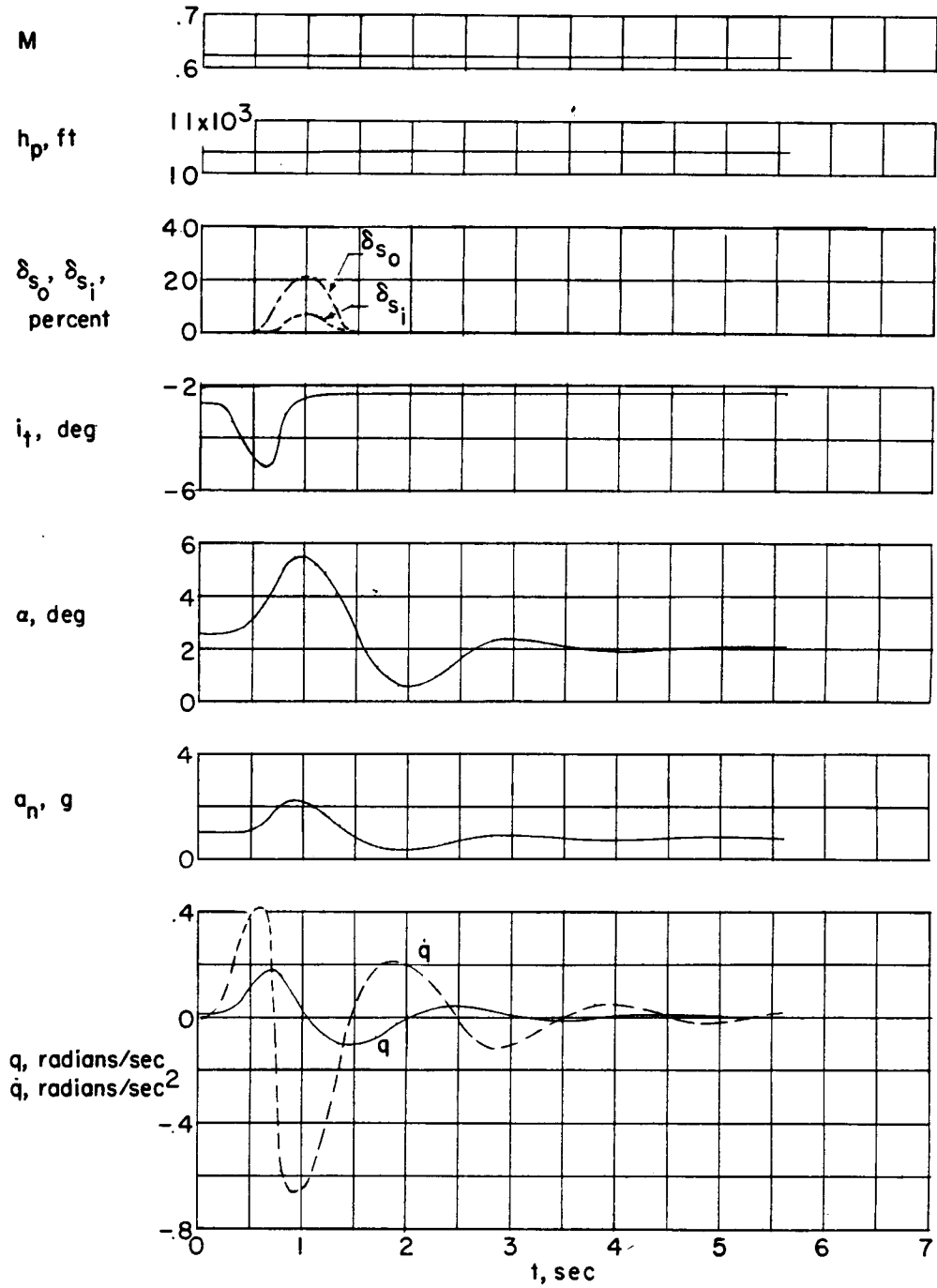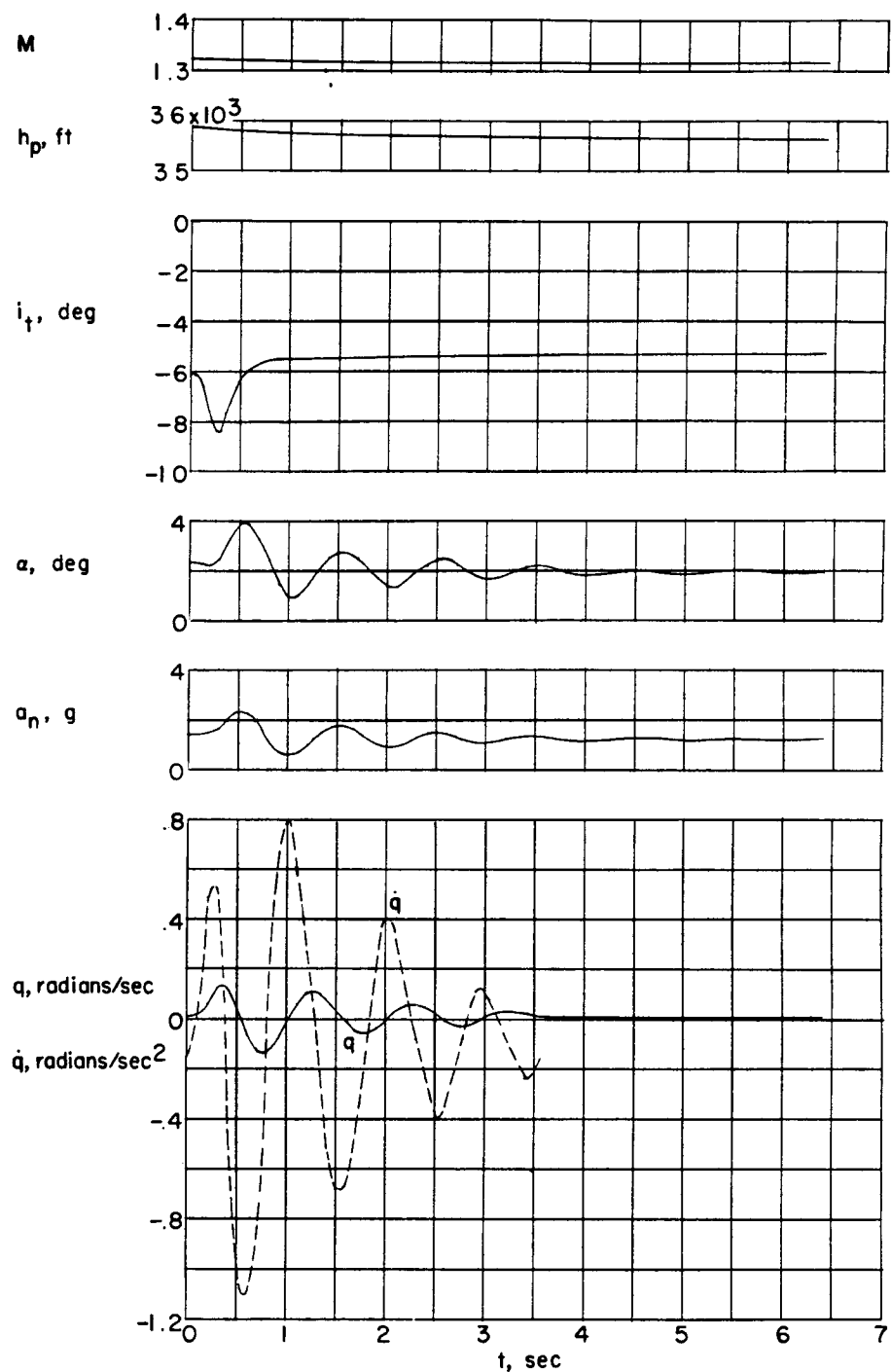
Figure 2.- Photograph of the airplane.

Figure 3.- Approximated variation of I_Y with weight. Clean configuration.

(a)   M = 0.62; h_p = 10,400 feet; extended-wing configuration.

Figure 4.- Time histories of longitudinal oscillations induced by a
stabilizer pulse.

(b)   M = 1.32; h_p = 35,700 feet; original-wing configuration.

Figure 4.- Concluded.
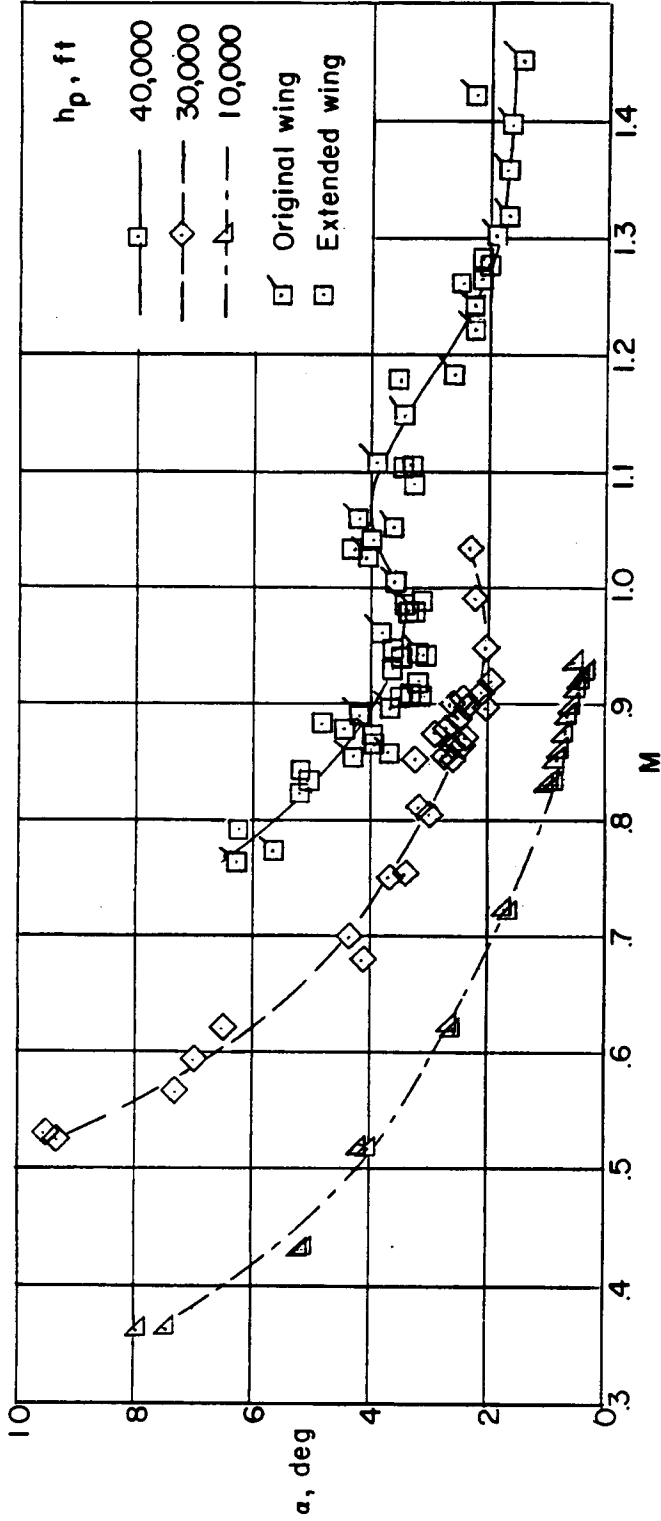
Figure 5.- Variation of trim angles of attack with Mach number.
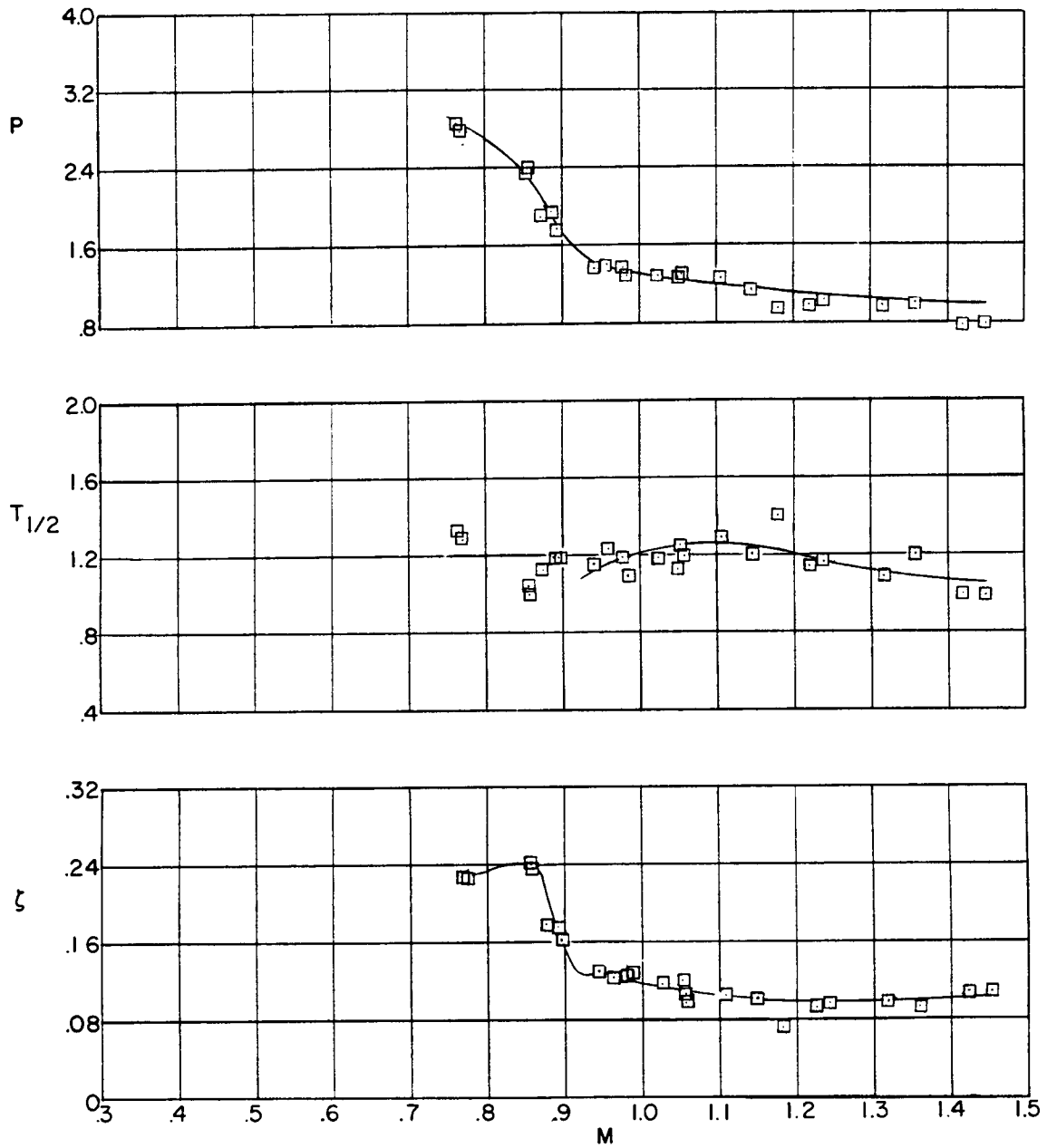
Figure 6.- Period and damping characteristics of the airplane as functions
of Mach number at 40,000 feet. Original-wing configuration.
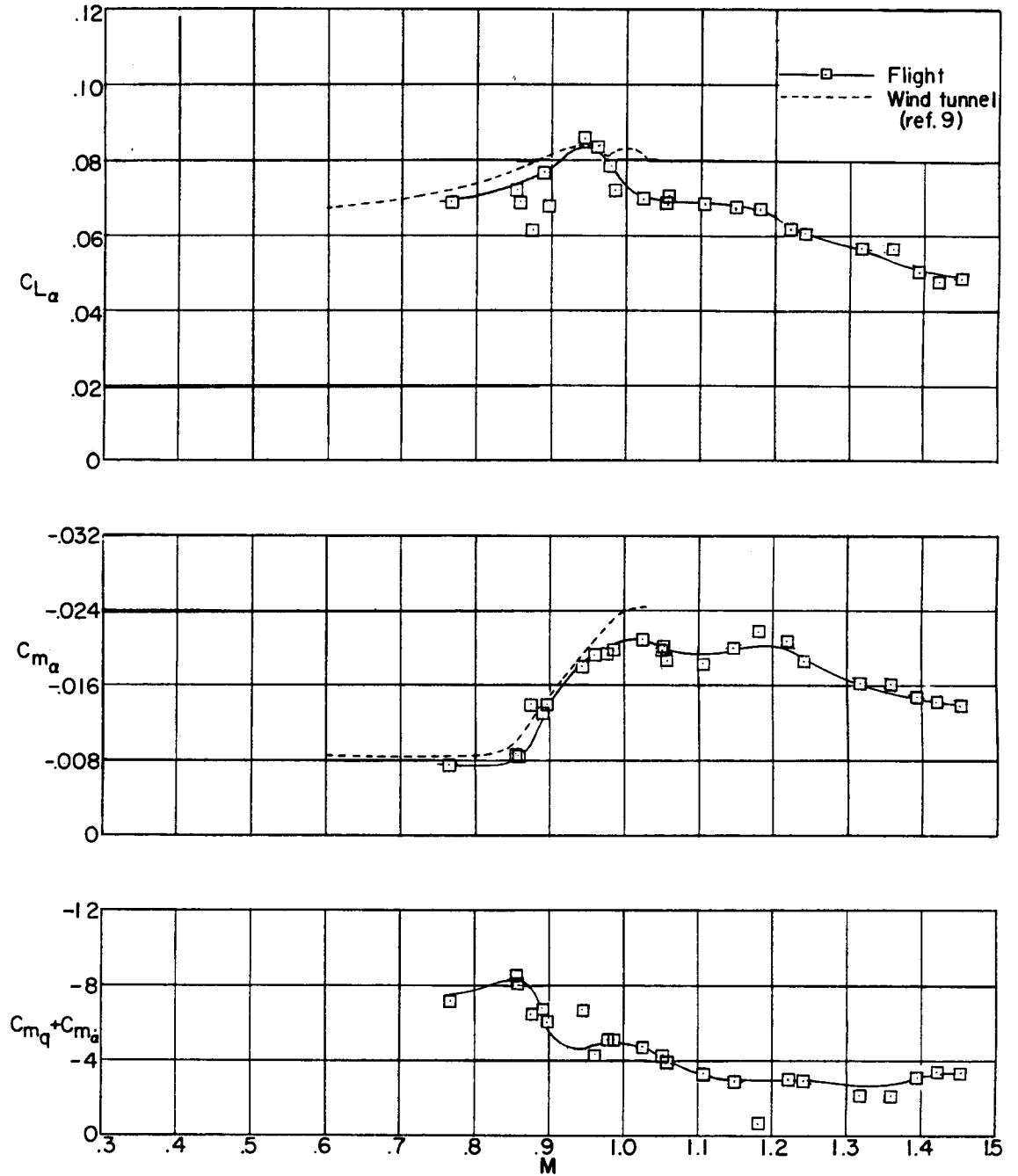
Figure 7.- Variation of static and dynamic longitudinal stability derivatives with Mach number at 40,000 feet. Original-wing configuration.
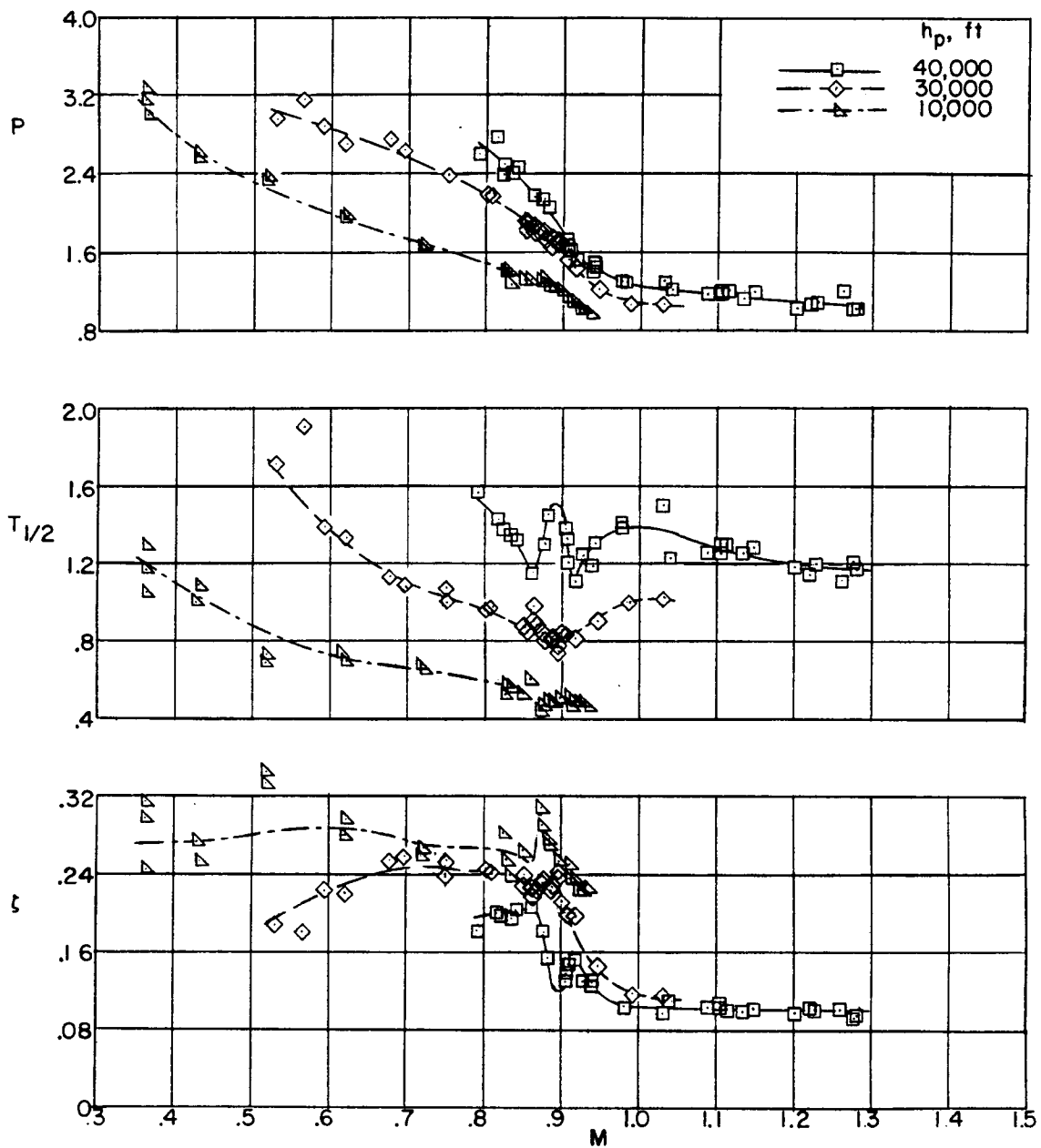
Figure 8.- Period and damping characteristics of the airplane at different
altitudes as functions of Mach number. Extended-wing configuration.
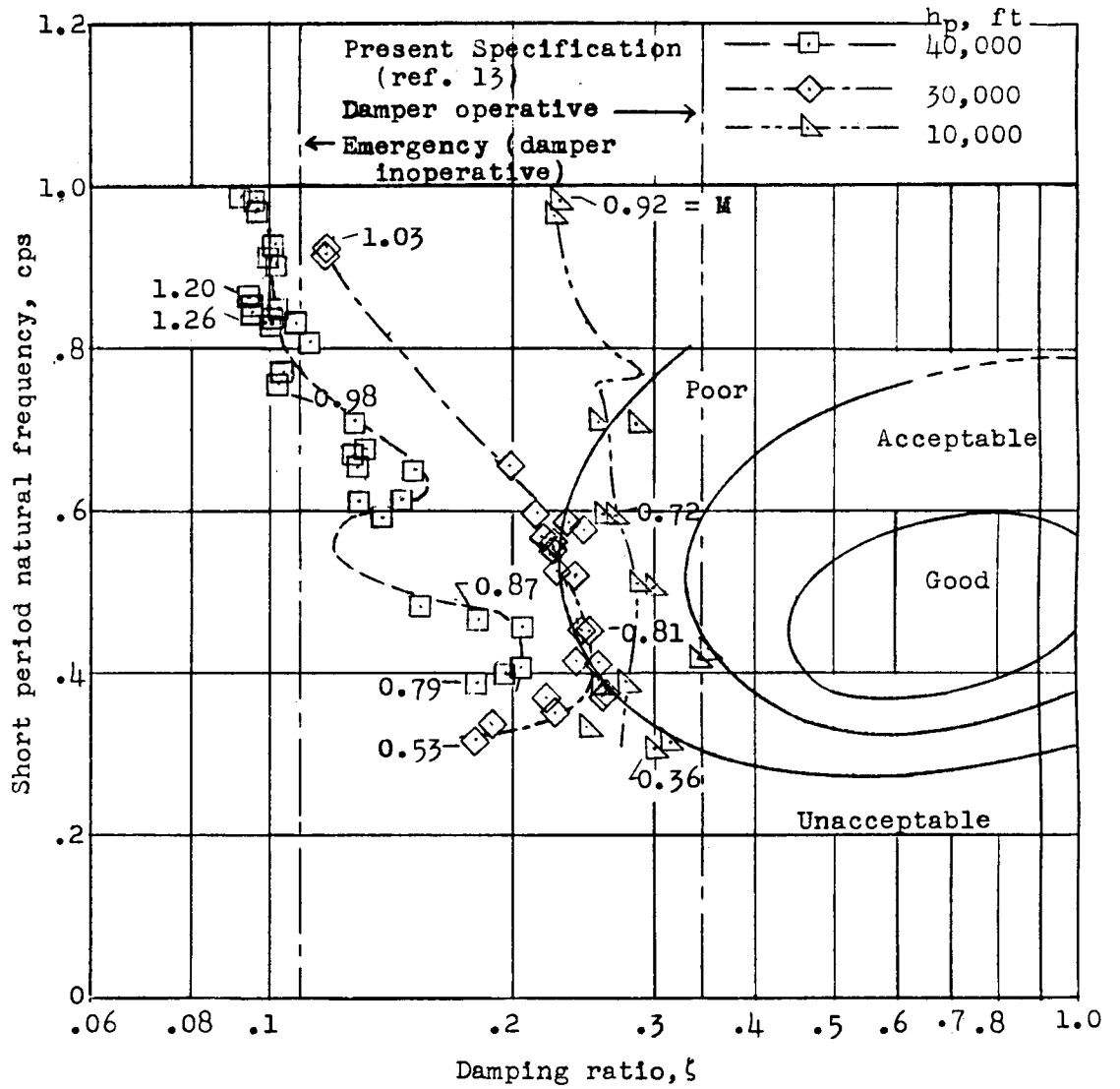
Figure 9.- Relation of flight-test results to qualitative rating criteria
of reference 12.

(a) C_{L_α}.

(b) C_{m_α}.
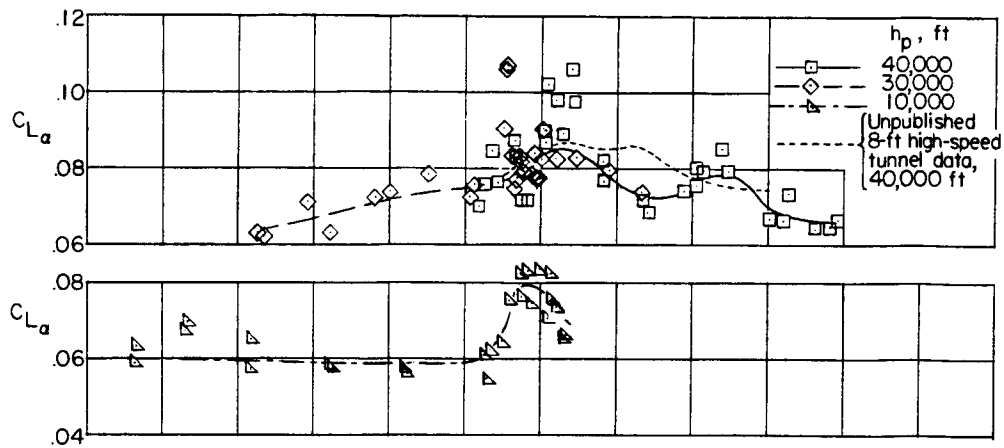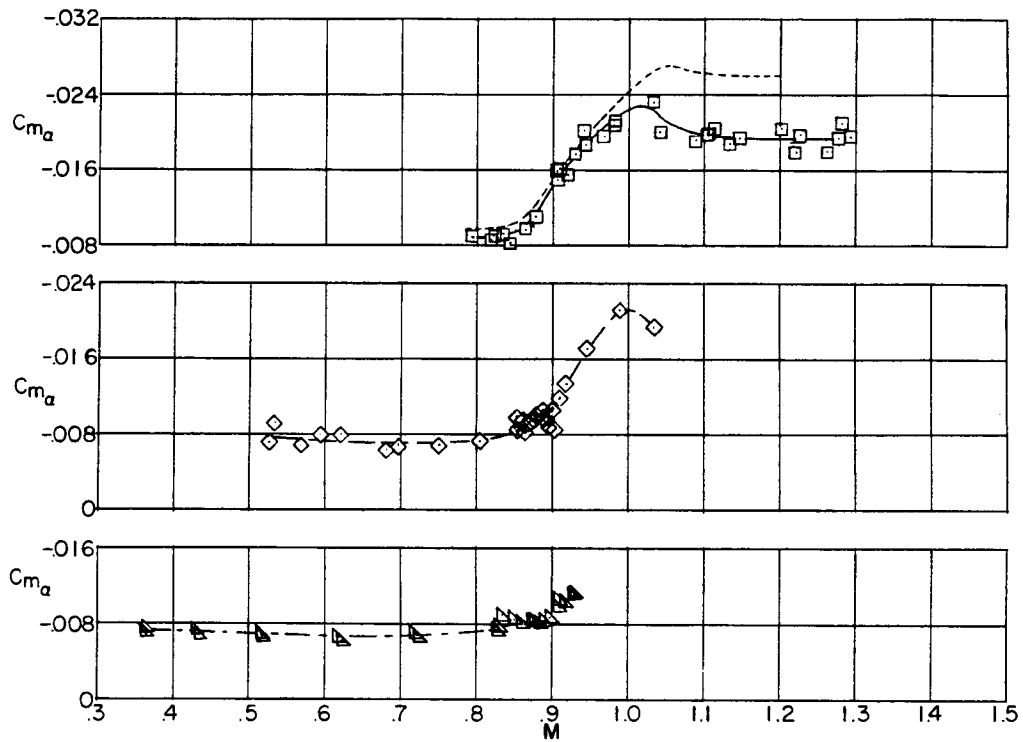
Figure 10.- Variation of static and dynamic longitudinal stability deriva-
tives with Mach number at different altitudes. Extended wing-tip
configuration.
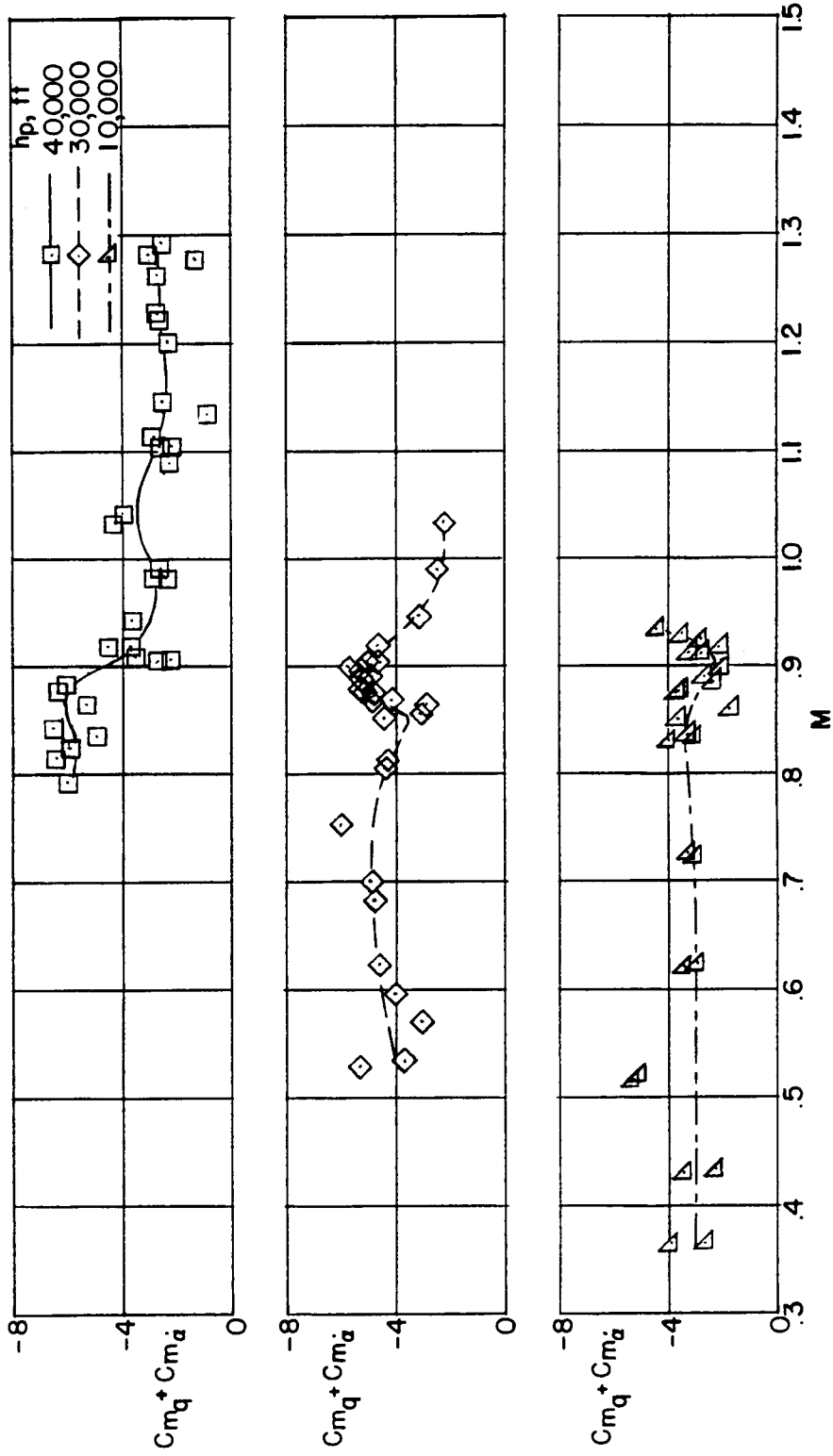
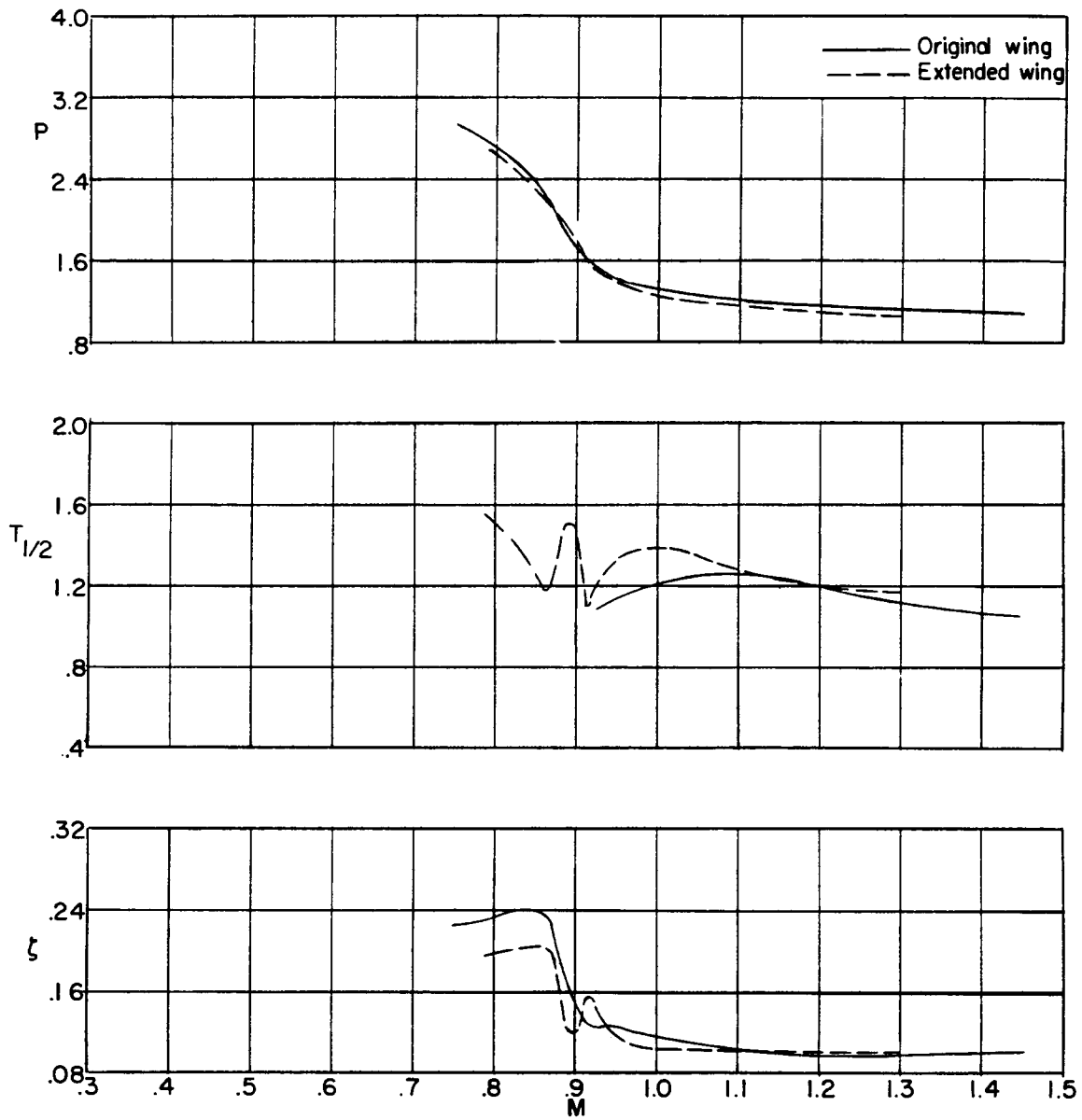(c) $C_{m_q} + C_{m_{\dot{\alpha}}}$.

Figure 10.- Concluded.

Figure 11.- Summary of the variation of period and damping characteristics of the two wing configurations with Mach number as determined from flight at 40,000 feet.
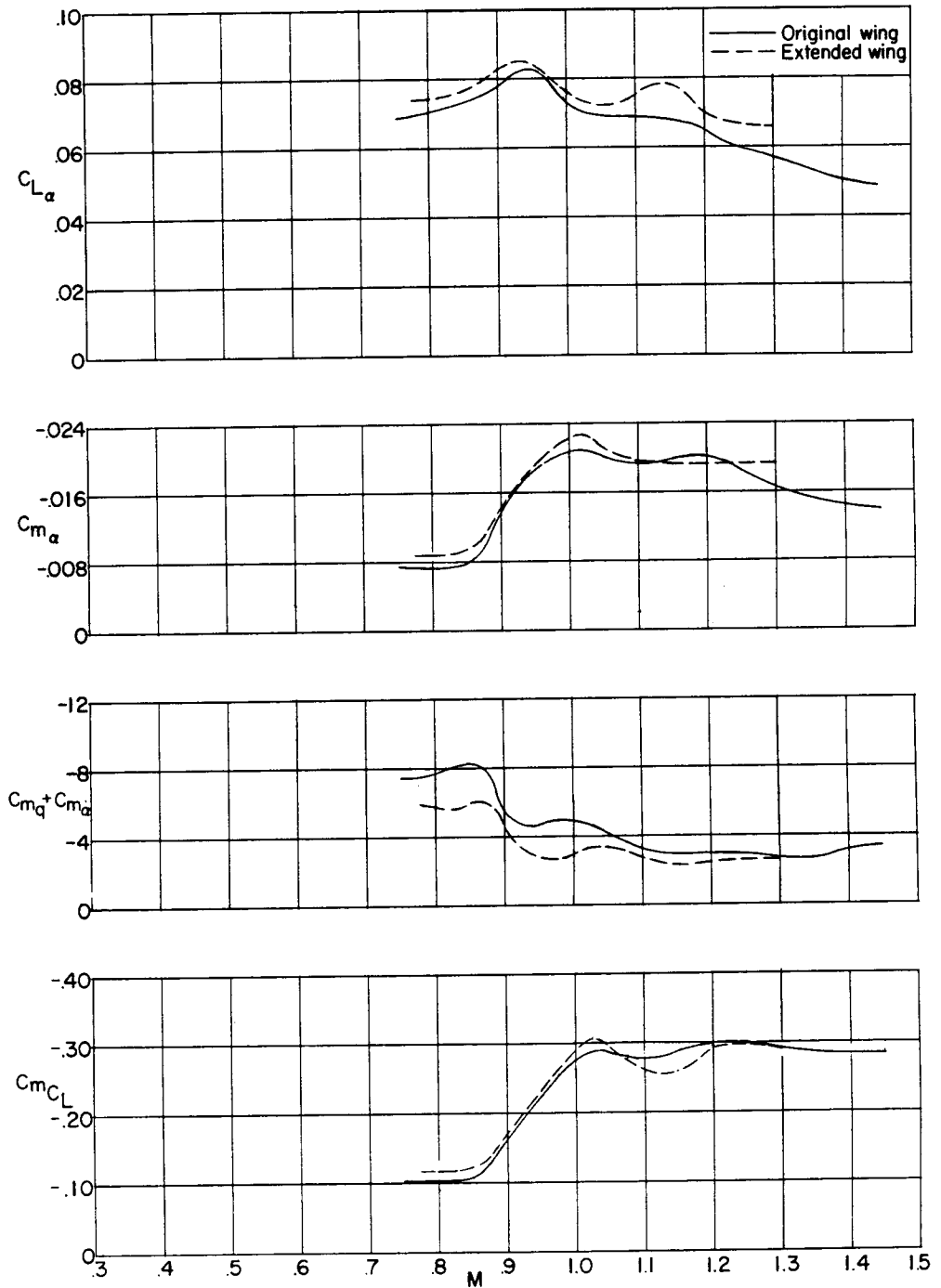
Figure 12.- Summary of the variation of the longitudinal stability derivatives of the two wing configurations with Mach number as determined from flight at 40,000 feet.